THE JOURNAL OF PHYSICAL CHEMISTRY C

Article

Cite This: J. Phys. Chem. C 2018, 122, 21162−21171

pubs.acs.org/JPCC

Effect of Chemical Composition and Crystal Phase of (Li,Na)FeO_2 Ferrites on CO_2 Capture Properties at High Temperatures

J. Francisco Gómez-García* and Heriberto Pfeiffer

Laboratorio de Fisicoquímica y Reactividad de Superficies (LaFReS), Instituto de Investigaciones en Materiales, Universidad Nacional Autónoma de México, Circuito exterior s/n, Cd. Universitaria, Del. Coyoacán, C. P. 04510 Ciudad de México, Mexico

ABSTRACT: In this work, we present the synthesis of lithium- and sodium-based ferrites by nitrate decomposition, using low and short thermal treatments. X-ray diffraction and Rietveld refinement were used to identify three different crystal phases: cubic, rhombohedral, and orthorhombic. By means of thermogravimetric experiments under CO_2 atmosphere, it was found that cubic-phase samples did not present an important CO_2 capture from 30 to 900 °C. However, rhombohedral and orthorhombic phases showed large capture properties at the same temperature range. The rhombohedral phase displayed a maximum CO_2 capture with 65% of expected capture (750 °C), while the orthorhombic phase showed 90% of the expected capture (700 °C). Additionally, the double exponential model, together with the Eyring model, were used to obtain rate constants and enthalpy of the activated states for CO_2 capture. From these data, a correlation of each capture process with the crystal structure and chemical composition was carried out. Finally, structural parameters together with electronegativity and hardness in chemical bonding were used to explain capture properties among the studied compositions.

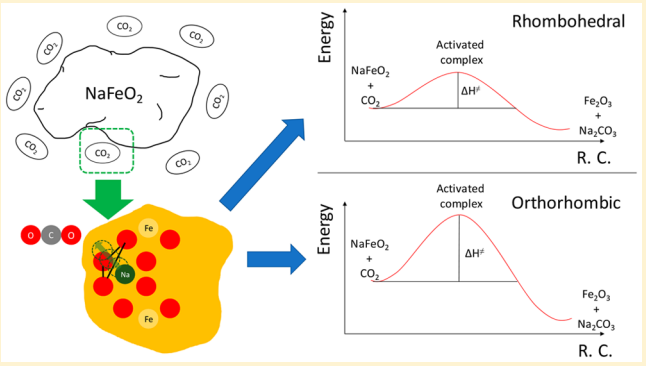

INTRODUCTION

Over the past years, due to the rising carbon dioxide (CO_2) levels in the atmosphere, the research community has focused on developing CO_2 capture technologies with a consequent increase in patents and research papers.[1] Most of these capture technologies are based on cryogenic distillation,[2,3] oxyfuel systems,[4,5] fuel cell systems,[6] ionic liquids,[7,8] and adsorption[2−4,8,9] or sorption processes.[2,3,5] In the last case, solid sorbents have been widely studied at low, moderate, and high temperatures[9] and in the presence of steam,[10−12] showing that alkali metal ceramics have good capture capabilities only at moderate and high temperature ranges.[13] Lithium- and sodium-based ceramics are particularly interesting for CO_2 capture at moderate and high temperatures in their native oxide forms,[14] as well as zirconates,[15−18] silicates,[19−21] cuprates,[22] aluminates,[23] and titanates,[24,25] among others.

Concerning CO_2 capture properties on lithium-based ferrites, it has been reported that Li_5FeO_4 has a maximum capture of 45 wt %,[26] while $LiFeO_2$ has been studied for CO_2 capture between 200 and 600 °C, showing small capture values below 500 °C.[27−29] Also, $LiFeO_2$ with alkali excess has been studied, showing a relation between CO_2 capture and alkali ion excess into the lattice.[30] Considering that alkali ions in crystal structures are mainly responsible for CO_2 capture properties, the study on (Li,Na)FeO_2 compounds has relevance due to a possible synergistic effect between CO_2 capture and different catalytic properties and applications, as has been already reported for different lithium-based ferrites.[31]

To our knowledge, $LiFeO_2$ compound crystallizes in a cubic close-packed arrangement of anions with cations located randomly in octahedral holes,[30] while the $NaFeO_2$ compound exhibits two crystal phases. α-$NaFeO_2$ presents a lattice with a rhombohedral crystal system in which oxygen anions form a close-packed-like array and cations are alternatively located in octahedral holes.[32] On the contrary, the β-$NaFeO_2$ crystal phase displays an orthorhombic crystal system, which can be described as a framework buildup of FeO_4 corner-linked tetrahedra. In this arrangement sodium ions are located in tetrahedral holes.[33] The α-$NaFeO_2$ phase is a low-temperature phase, whereas the β-$NaFeO_2$ phase is stable above 750 °C.[34] There are two other polymorphs with $NaFeO_2$ chemical composition, but these are not of interest in this work due to their stabilization conditions. The γ-$NaFeO_2$ phase prevails above 1000 °C, and the δ-$NaFeO_2$ phase appears above 1250 °C.[34]

In this context, the aim of this work was to synthesize several compositions that belong to the $Li_{1-x}Na_xFeO_2$ system, in order to correlate their CO_2 capture properties with their chemical composition and structural characteristics.

EXPERIMENTAL SECTION

$Li_{1-x}Na_xFeO_2$ ($0 < x < 1$) compounds were synthesized by the nitrate decomposition route. Stoichiometric amounts of lithium

Received: June 11, 2018
Revised: August 23, 2018
Published: August 27, 2018

DOI: 10.1021/acs.jpcc.8b05578
J. Phys. Chem. C 2018, 122, 21162−21171

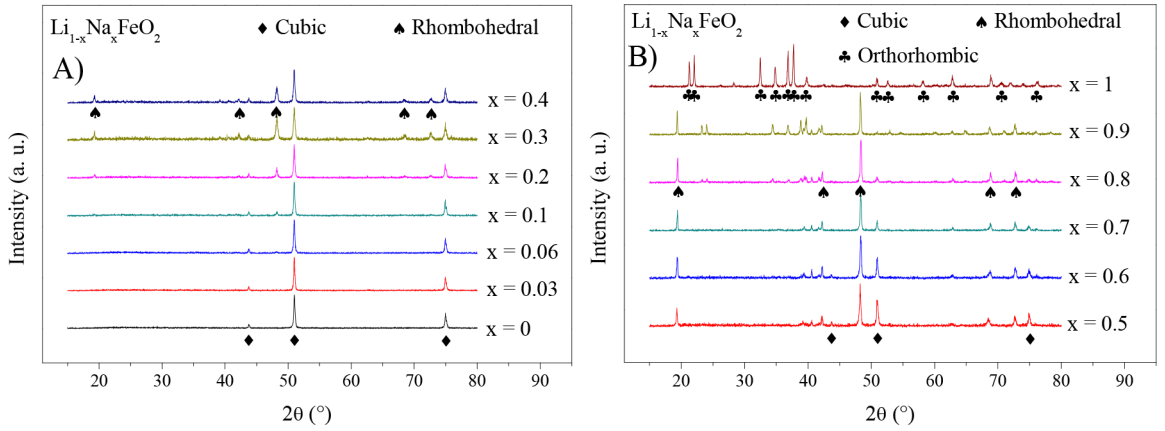

Figure 1. X-ray diffraction patterns for all synthesized samples.

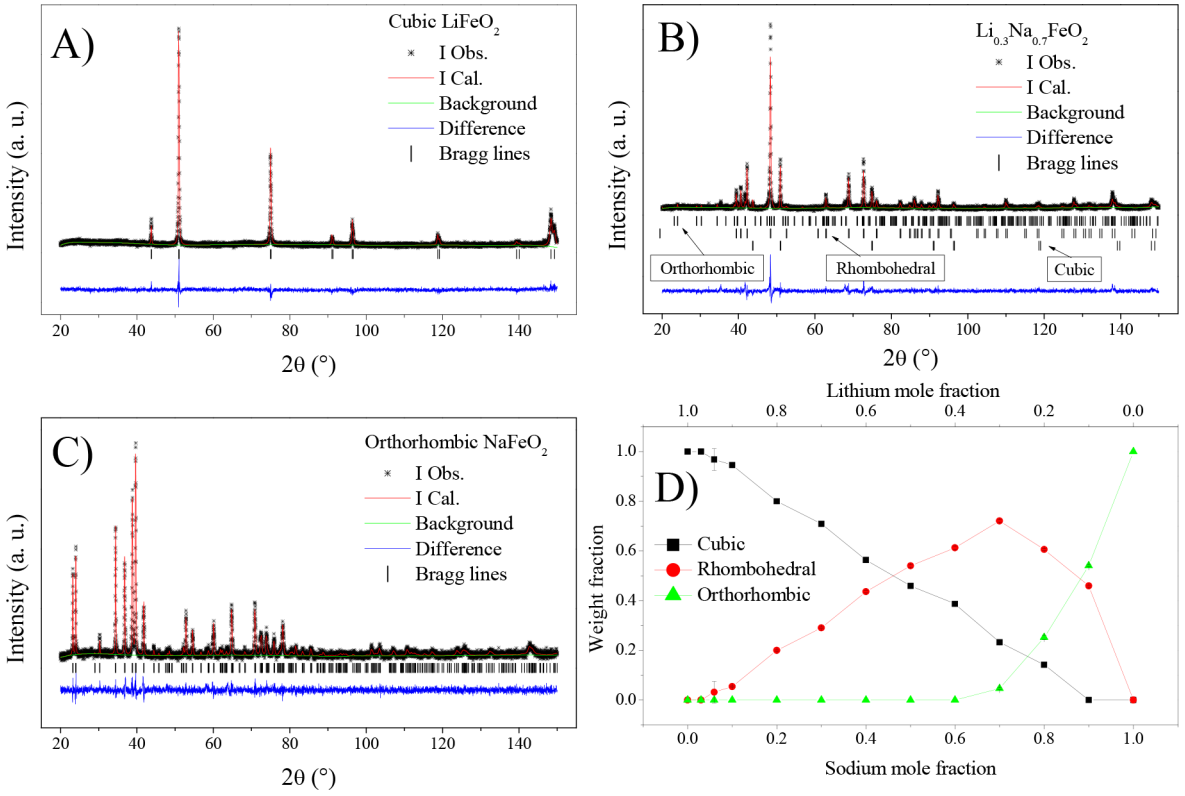

Figure 2. Rietveld refinement plots for: (A) $LiFeO_2$, (B) $Li_{0.3}Na_{0.7}FeO_2$, and (C) $NaFeO_2$ nominal compositions. (D) Phase composition in the whole system. At small sodium content values there is a solid solution with cubic crystal phase.

carbonate, sodium carbonate, and ferric nitrate ninth-hydrated (all supplied by Meyer 99.9%) were weighted according to eq 1. The reagents were mixed and dissolved in distilled water, and then HNO_3 (Sigma-Aldrich 99%) was added dropwise until the total alkali carbonate reaction. The solution was heated to dryness, and the remaining solid was pyrolyzed at 500 °C for 3 h in air atmosphere. Finally, a precursor was annealed at 800 °C for 1 h in air atmosphere.

$$\left(\frac{1-x}{2}\right)Li_2CO_3 + \left(\frac{x}{2}\right)Na_2CO_3 + Fe(NO_3)_3\cdot 9H_2O \rightarrow Li_{1-x}Na_xFeO_2 + CO_2 + 3NO_x \quad (1)$$

The crystal structure characterization of synthesized compositions was carried out by X-ray diffraction in a Siemens D5000 diffractometer coupled with a Co K_α anode (λ = 1.789 Å) and scintillation counter. Further Rietveld refinement was performed on each X-ray pattern using the GSAS code[35] with EXPGUI interface.[36]

CO_2 capture evaluation was performed in a TA Instruments Q500HR thermobalance using dynamic and isothermal conditions. All experiments were performed under 60 mL/min CO_2 flow (Praxair 3.0 grade). Dynamic experiments were performed on 30 mg of samples between 30 and 900 °C with a heating rate of 10 °C/min. Isothermal experiments were done with 90 mg of samples and were heated under an inert atmosphere (60 mL/min flow of N_2 Praxair 4.8 grade) up to a stable state at target temperature, and then gas flow was switched to CO_2. Under these conditions weight data were collected for 180 min. CO_2 capture cycling experiments were carried out in a

DOI: 10.1021/acs.jpcc.8b05578
J. Phys. Chem. C 2018, 122, 21162−21171

TA Instruments Q550 themobalance with 90 mg of sample. The CO_2 capture process was done under CO_2 flow (60 mL/min) at 600 °C for 2 h, while the decarbonation process was done under N_2 flow (60 mL/min) at 800 °C for 30 min. Cyclic experiment products were characterized by X-ray diffraction and N_2 adsorption−desorption in a Bel-Japan Minisorp II at 77 K; an additional Brunauer−Emmet−Teller (BET) model was employed to obtain specific surface area. Temperature-programmed desorption (TPD) analyses were done to identify CO_2 desorption processes. TPD experiments were carried out in a chemisorption analyzer Belcat, Bel-Japan, coupled with a thermal conductivity detector (TCD). Before TPD experiments, each sample was pretreated by heating it to 850 °C in a helium flow (30 mL/min Praxair 4.7 grade) for 1 h. Then the temperature was fixed to 700 °C, and a 60 mL/min CO_2 flow was passed through the cell for 1 h to saturate the sample. After pretreatment, TPD analysis was performed between 80 and 900 °C at 5 °C/min of heating rate in helium flow (30 mL/min).

RESULTS AND DISCUSSION

The compositions synthesized presented a progressive color change from orange for lithium-rich samples to brown for sodium-rich samples. X-ray diffraction patterns (Figure 1) showed a single-crystal phase only for $LiFeO_2$, $Li_{0.97}Na_{0.03}FeO_2$, $Li_{0.94}Na_{0.06}FeO_2$, and $NaFeO_2$ samples. Lithium-based compositions displayed characteristic patterns for face cubic centered lattice with $Fm\bar{3}m$ space group (SG).[30] However, the $NaFeO_2$ composition presented a characteristic pattern for a primitive lattice with orthorhombic crystal system and $Pna2_1$ SG.[37] The remaining compositions showed X-ray diffraction patterns with two or three different crystal phases, including a rhombohedral lattice similar to the α-$NaFeO_2$ phase reported by McQueen et al.[38]

Based on that, Rietveld refinements were performed on all diffraction patterns. Figures 2A, 2B, and 2C display Rietveld refinement plots for $LiFeO_2$, $Li_{0.3}Na_{0.7}FeO_2$, and $NaFeO_2$ compositions, respectively. Also, the behavior of weight fraction of different crystal phases is presented in Figure 2D. It is possible to observe that the cubic phase was the only crystal phase present in samples with high lithium content ($LiFeO_2$, $Li_{0.97}Na_{0.03}FeO_2$, and $Li_{0.94}Na_{0.06}FeO_2$). The rhombohedral phase took place at compositions between 0.1 and 0.9 mol % of sodium. This phase reached a maximum content on $Li_{0.3}Na_{0.7}FeO_2$ nominal composition with 0.75 wt %, as well as 0.04 of orthorhombic phase and 0.21 of cubic phase. At higher sodium contents, the rhombohedral phase decreased, while the orthorhombic phase took place in the system. On 100 mol % of Na composition, the orthorhombic phase was the only crystal phase presented. Additionally, in Figure 2D it was possible to observe a linear decrement of the cubic phase, while sodium content increased which could imply that both phases did not form a solid solution system. Along with this behavior, the rhombohedral phase fraction decreased when sodium contents were higher than 70%. In the same region, the orthorhombic phase took place in the diagram, increasing its weight fraction, while the rhombohedral phase vanished. Additionally, structural and atomic parameters obtained from Rietveld refinements are listed in Tables 1 and 2.

According to Figure 2D, compositions with small sodium content ($x < 0.06$) only displayed a cubic phase. Therefore, thermogravimetric CO_2 capture studies were performed initially on $LiFeO_2$, $Li_{0.97}Na_{0.03}FeO_2$, and $Li_{0.94}Na_{0.06}FeO_2$ samples to evaluate sodium influence on CO_2 capture properties in the cubic phase (Figure 3). The $LiFeO_2$ sample showed a weight gain (1.6 wt %) at 490 °C, and CO_2 capture was significant from 300 °C. Several alkali-based oxides display a slight CO_2 capture between 200 and 500 °C before a second and largest capture. This behavior is associated with a double-stage capture process: at low temperatures ($T < 500$ °C) CO_2 capture takes place by surface interactions. At $T > 500$ °C ion diffusion increases considerably, and CO_2 capture occurs by bulk interactions.[14,39,40] Consequently, the weight increment showed by the $LiFeO_2$ sample was associated with a CO_2 surface capture. At $T > 500$ °C a weight loss took place indicating a complete superficial decarbonation. Moreover, samples with $x = 0.03$ and $x = 0.06$ values displayed a maximum CO_2 capture of 1.15 and 1.34 wt %, respectively; these values were slightly smaller than

Table 1. Crystal Structure Parameters for (Li,Na)FeO_2 Ferrites

parameter	cubic phase	rhombohedral phase	orthorhombic phase
space group (no.)	$Fm\bar{3}m$ (225)	$R\bar{3}m$ (166)	$Pna2_1$ (33)
lattice parameters (Å)	a = 4.1572(6)	a = 3.0172(1)	a = 5.6661(2)
			b = 7.1475(2)
		c = 15.9163(9)	c = 5.3830(2)
volume (Å^3)	71.848(4)	125.48(1)	218.01(2)
Z	2	3	4

Table 2. Atomic Positions and Site Occupation Factors (S.O.F.) for Crystal Phases Presented by (Li,Na)FeO_2 Ferrites

crystal phase	crystallographic atom	x/a	y/b	z/c	S.O.F.
cubic	Li	0	0	0	0.5
	Fe	0	0	0	0.5
	O	1/2	1/2	1/2	1.0
rhombohedral	Na	0	0	0	1.0
	Fe	0	0	1/2	1.0
	O	0	0	0.235	1.0
orthorhombic	Na	0.428	0.120	0.470	1.0
	Fe	0.069	0.129	0.466	1.0
	O(1)	0.036	0.099	0.344	1.0
	O(2)	0.374	0.170	0.911	1.0

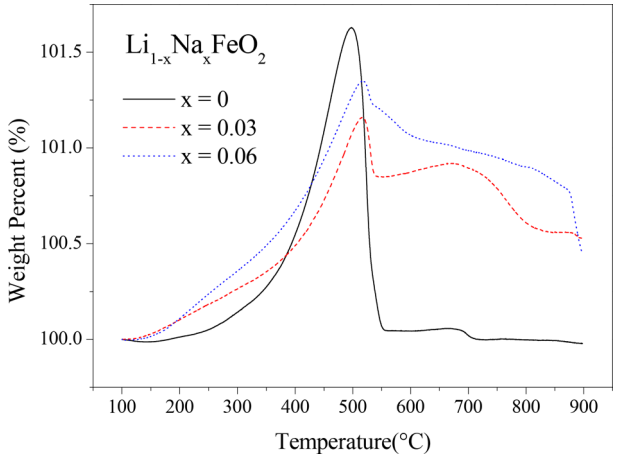

Figure 3. Dynamic thermogravimetric experiments performed on $LiFeO_2$, $Li_{0.97}Na_{0.03}FeO_2$, and $Li_{0.94}Na_{0.06}FeO_2$ samples under CO_2 atmosphere.

DOI: 10.1021/acs.jpcc.8b05578
J. Phys. Chem. C 2018, 122, 21162−21171

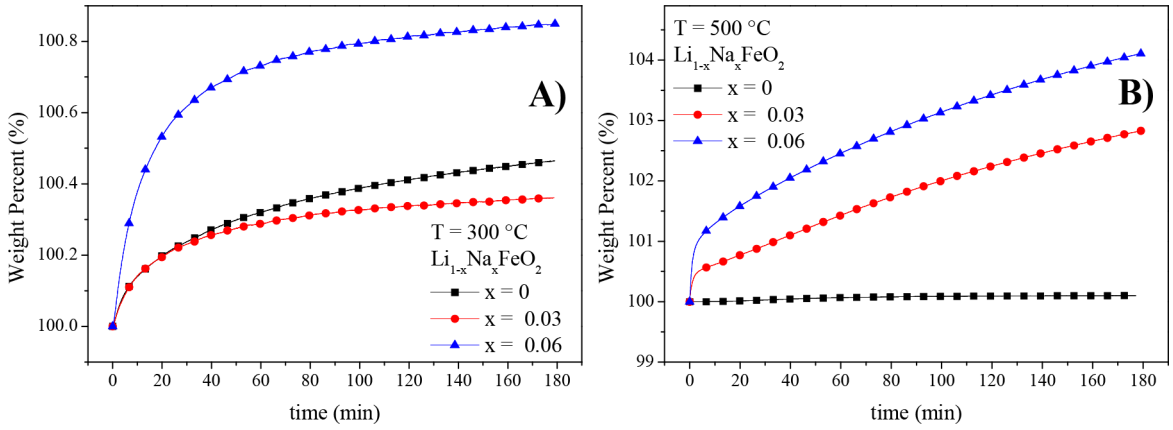

Figure 4. Isothermal thermogravimetric experiments for $LiFeO_2$, $Li_{0.97}Na_{0.03}FeO_2$, and $Li_{0.94}Na_{0.06}FeO_2$ samples under CO_2 atmosphere at (A) 300 °C and (B) 500 °C.

the one displayed by the $LiFeO_2$ sample. However, in both compositions, the surface decarbonation process took place at 520 °C. This increment in the decarbonation temperature was related to a possible surface modification by sodium addition. In fact, not only the decarbonation temperature was modified in these Na-doped samples but also the temperature in which the CO_2 capture began. In both doped samples, the CO_2 capture process started at 175 °C, which was 125 °C lower than that displayed by $LiFeO_2$ sample.

Unlike $LiFeO_2$, the superficial decarbonation process in $Li_{0.97}Na_{0.03}FeO_2$ and $Li_{0.94}Na_{0.06}FeO_2$ samples was not completed, and a remnant weight lasted until 860 °C. In fact, a second decarbonation process was observed for $Li_{0.94}Na_{0.06}FeO_2$ at higher temperatures, which was related to sodium carbonate decomposition. The presence of both lithium and sodium carbonates on $Li_{0.97}Na_{0.03}FeO_2$ and $Li_{0.94}Na_{0.06}FeO_2$ samples could be related to the weight losses shown in Figure 3. Although CO_2 capture was improved by sodium addition in cubic $LiFeO_2$ at $T > 550$ °C, the maximum capture displayed by Na-doped samples was considerably lower than 23 wt %, which is the expected CO_2 capture for $LiFeO_2$, considering eq 2.

$$2LiFeO_2 + CO_2 \rightarrow Fe_2O_3 + Li_2CO_3 \quad (2)$$

Additionally to dynamic thermogravimetric experiments, isothermal experiments were carried out to elucidate kinetics related to CO_2 capture in these compositions. Figure 4 shows two sets of isothermal experiments for $LiFeO_2$, $Li_{0.97}Na_{0.03}FeO_2$, and $Li_{0.94}Na_{0.06}FeO_2$ samples at 300 and 500 °C. Experiments performed at 300 °C showed a small CO_2 capture after 180 min (Figure 4A). The $Li_{0.94}Na_{0.06}FeO_2$ sample displayed the higher CO_2 capture (0.8 wt %), which was related to sodium content. Moreover, at this temperature, the $Li_{0.97}Na_{0.03}FeO_2$ sample showed less CO_2 capture than $LiFeO_2$. Perhaps, at this temperature chemical composition was not enough to significantly enhance the CO_2 capture, and only superficial capture was mainly responsible in both compounds.

Figure 4B shows isothermal experiments for $LiFeO_2$, $Li_{0.97}Na_{0.03}FeO_2$, and $Li_{0.94}Na_{0.06}FeO_2$ samples performed at 500 °C. The null CO_2 capture displayed by the $LiFeO_2$ sample is remarkable, which agreed with the decarbonation process displayed in dynamic experiments. Otherwise, $Li_{0.97}Na_{0.03}FeO_2$ and $Li_{0.94}Na_{0.06}FeO_2$ samples displayed CO_2 capture capabilities proportional to sodium content: 2.8 and 4.1 wt %, respectively. The profile depicted by isothermal CO_2 capture at 300 °C suggests that the reaction was almost completed in each sample, but at 500 °C it did not occur (see Figure 4). This characteristic indicated a different capture process at this temperature. Bearing this hypothesis in mind, isothermal experiments at the 250−500 °C temperature range were performed. Time-dependent data were processed taking into account the double exponential model which represented two independent capture processes with different rate constants (k_1 and k_2, min^{-1})[16,41] as in eq 3.

$$\begin{aligned} &2(Li, Na)FeO_2 + CO_2 \\ &\xrightarrow{k_1} Fe_2O_3 + ((Li, Na)_2CO_3)_{surface} \\ &\xrightarrow{k_2} Fe_2O_3 + ((Li, Na)_2CO_3)_{bulk} \end{aligned} \quad (3)$$

The weight percentage gain with time evolution was well described by the double exponential model (eq 4), wherein A and B are CO_2 capture capability (in weight percentage) for each process and C is the total CO_2 amount captured by the material plus the initial sample weight. In this case $C = A + B + 100\%$, 100% was taken as the initial sample weight percent.

$$wt\ \% = -A\exp(-k_1 t) - B\exp(-k_2 t) + C \quad (4)$$

In addition to double exponential model fit, rate constants obtained were treated under the Eyring model to calculate the activated-state enthalpy ($\Delta H^{\ddagger}$).[41] The Eyring model takes into account an activated state where not only the momentum transfer and symmetry orientation matter but also vibrational states as well as tunneling effect were used to calculate the potential surfaces to describe the activated state, for which kinetic energy was quantized by the position in the potential surface.[42−44] The Eyring formulation is presented in eq 5, where R is the ideal gas constant, k_B the Boltzmann constant, h the Planck constant; and $\Delta S^{\ddagger}$ is the activated-state entropy associated with the CO_2 capture process.

$$\ln\left(\frac{k}{T}\right) = -\left(\frac{\Delta H^{\ddagger}}{R}\right)\left(\frac{1}{T}\right) + \ln\left(\frac{k_B}{h}\right) + \frac{\Delta S^{\ddagger}}{R} \quad (5)$$

Figure 5 shows the calculated rate constants under Eyring treatment, and it could be seen that rate constants associated with the k_2 process (open symbols in Figure 5) had the same behavior for the studied samples. According to X-ray diffraction patterns, these compounds had the same crystal structure; therefore, k_2 values could be related with a CO_2 capture process, in which a bulk-diffusional effect was mainly responsible for this process.

DOI: 10.1021/acs.jpcc.8b05578
J. Phys. Chem. C 2018, 122, 21162−21171

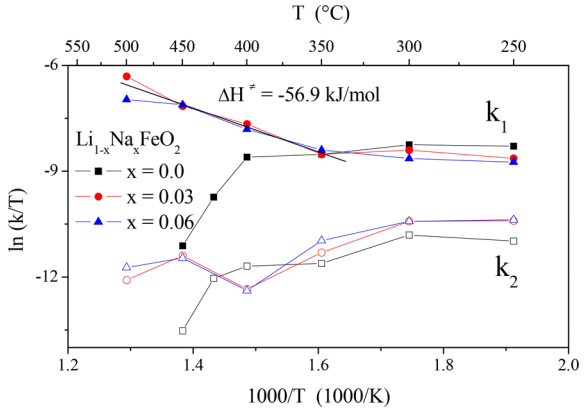

Figure 5. Eyring-type plots for CO_2 capture rate constants in $LiFeO_2$, $Li_{0.97}Na_{0.03}FeO_2$, and $Li_{0.94}Na_{0.06}FeO_2$ samples.

Otherwise, k_1 values (filled symbols in Figure 5) had two different behaviors: one with a positive slope for the $LiFeO_2$ sample, and thus, there was no physical meaning to estimate $\Delta H^{\ddagger}$. The second behavior yielded a negative slope, so it was possible to estimate a $\Delta H^{\ddagger}$ = 56.9 kJ/mol between 350 and 500 °C for $Li_{0.97}Na_{0.03}FeO_2$ and $Li_{0.94}Na_{0.06}FeO_2$ samples. This difference between the $LiFeO_2$ sample and Na-based compounds could be correlated with their chemical composition. In this way, the calculated $\Delta H^{\ddagger}$ represents a sodium-dependent process, which agreed with surface CO_2 capture. Additionally, it was expected that, in doped systems (as $Li_{0.97}Na_{0.03}FeO_2$ and $Li_{0.94}Na_{0.06}FeO_2$ samples where Na ions replace Li ions), defect concentration should be high at the particle surface. In such a case, CO_2 capture could be favored by Na_2CO_3 formation instead of Li_2CO_3 for which formation was not suitable on the cubic $LiFeO_2$ sample.[30]

Concerning the k_2 rate constant process, it could be seen that it involves a slow CO_2 capture; additionally, in Figure 5 the k_2 values display similar behavior between them despite the different chemical composition. Thus, k_2 values could be correlated with the crystal structure which is the same for these three samples. In this scenario, bulk diffusion processes could be responsible for CO_2 capture. The fact that k_2 values diminish with the temperature is against a thermally activated diffusion process, but the Eyring model considers different aspects to model the potential surface. Thus, bulk diffusion could not be the only process involved in bulk capture. Additional to the diffusion process, intensity in lattice vibrations (phonons) increased with temperature; in consequence, it could be possible that CO_2 capture in the cubic $LiFeO_2$ sample was not favored due to phonon energy. Therefore, the kinetic rate became lower as the temperature increased. However, for Na-containing samples it was possible to obtain a $\Delta H^{\ddagger}$ = 56.9 kJ/mol, which was similar to that calculated for other Na-containing ceramics, e.g., 48 kJ/mol for Na_2ZrO_3,[16] 23.9 kJ/mol for Na_2SiO_3,[19] 30.6 kJ/mol for $Na_2Zr_{0.7}Al_{0.3}O_3$,[40] and 21.6 kJ/mol for Na_2TiO_3.[24]

CO_2 capture properties in high sodium-containing samples were performed, at first, by dynamic thermogravimetric analysis on $NaFeO_2$ and some $Li_{1-x}Na_xFeO_2$ samples. These results are shown in Figure 6, where it could be seen that the $NaFeO_2$ sample had a maximum CO_2 capture of 15.2 wt % at 790 °C, which represented near 75% of the expected capture (19.9 wt % according to eq 6). Additionally, the CO_2 capture profile depicted by the $Li_{0.1}Na_{0.9}FeO_2$ sample was similar to the

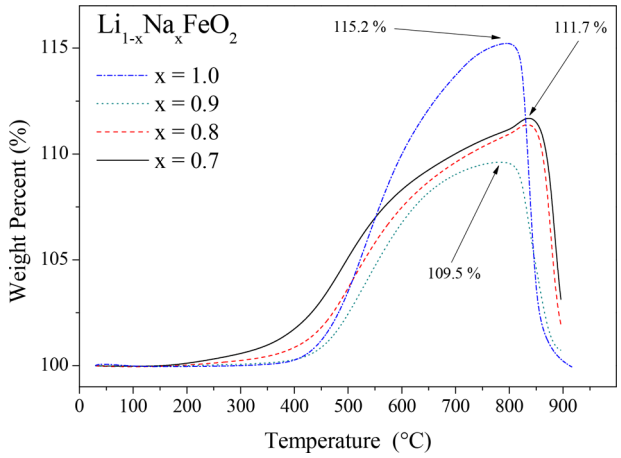

Figure 6. Dynamic thermogravimetric results for $NaFeO_2$, $Li_{0.1}Na_{0.9}FeO_2$, $Li_{0.2}Na_{0.8}FeO_2$, and $Li_{0.3}Na_{0.7}FeO_2$ samples under CO_2 atmosphere.

$NaFeO_2$ profile. Moreover, the CO_2 capture in $Li_{0.1}Na_{0.9}FeO_2$ dropped to 9.5 wt % which corresponds to 37.5% less CO_2 capture than that presented by the $NaFeO_2$ sample. This ratio correlates with orthorhombic weight fraction presented in $Li_{0.1}Na_{0.9}FeO_2$ composition (near 60% in Figure 2D). In this way, CO_2 capture displayed by the $Li_{0.1}Na_{0.9}FeO_2$ sample could be produced due to the orthorhombic crystal phase.

$$2NaFeO_2 + CO_2 \rightarrow Fe_2O_3 + Na_2CO_3 \quad (6)$$

Furthermore, $Li_{0.2}Na_{0.8}FeO_2$ and $Li_{0.3}Na_{0.7}FeO_2$ samples were studied by dynamic thermogravimetry. In Figure 6 it could be seen that these compositions displayed maximum CO_2 captures around 11.7 wt % at 850 °C, which were higher than that presented by the $Li_{0.1}Na_{0.9}FeO_2$ sample. Moreover, not only maximum CO_2 capture changed but also the dynamical thermogravimetric profile was depicted. For $Li_{0.2}Na_{0.8}FeO_2$ and $Li_{0.3}Na_{0.7}FeO_2$ compositions, CO_2 capture began at 250 °C, which was almost 150 °C lower than in the 90 and 100% sodium compositions. Also, these compounds presented a maximum CO_2 capture 60 °C above the $NaFeO_2$ sample. To compare these thermogravimetric analyses, derivative thermogravimetric plots (DTGs) are presented in Figure 7, where a

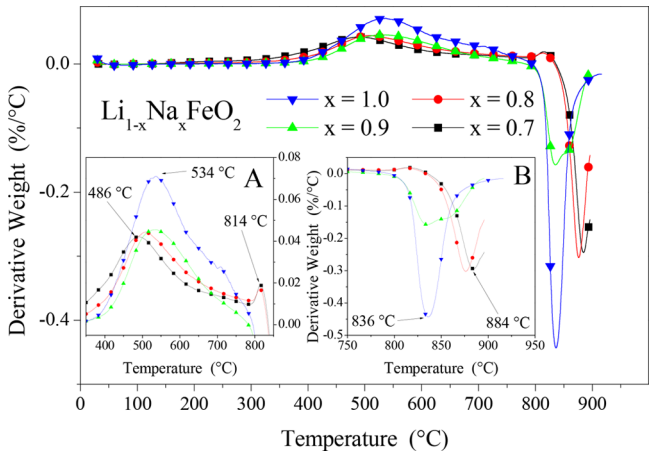

Figure 7. Derivative thermogravimetric analysis for $NaFeO_2$, $Li_{0.1}Na_{0.9}FeO_2$, $Li_{0.2}Na_{0.8}FeO_2$, and $Li_{0.3}Na_{0.7}FeO_2$ samples under CO_2 atmosphere. (A) Capture interval and (B) decarbonation interval.

DOI: 10.1021/acs.jpcc.8b05578
J. Phys. Chem. C 2018, 122, 21162−21171

capture process with a positive derivate in the inset A can be observed. In this graph can be seen a maximum CO_2 capture rate at 534 °C for $NaFeO_2$ and $Li_{0.1}Na_{0.9}FeO_2$ samples, but this value decreased to 486 °C for the $Li_{0.3}Na_{0.7}FeO_2$ sample. $Li_{0.2}Na_{0.8}FeO_2$ and $Li_{0.3}Na_{0.7}FeO_2$ compositions also presented a second maximum capture rate at 814 °C, which were not present in higher sodium-containing compositions. These characteristics would be related to the rhombohedral crystal phase, which was the majority crystal phase in $Li_{0.2}Na_{0.8}FeO_2$ and $Li_{0.3}Na_{0.7}FeO_2$ samples (see Figure 2D).

Figure 7B displays a negative derivate associated with decarbonation. At first sight, it is possible to observe a maximum decomposition rate at 836 °C for the $NaFeO_2$ sample, which shifted progressively to higher temperatures (884 °C), while sodium content decreased. This characteristic could be correlated with the presence of the rhombohedral crystal phase in $Li_{0.2}Na_{0.8}FeO_2$ and $Li_{0.3}Na_{0.7}FeO_2$ nominal compositions. To elucidate the decarbonation process in these samples, CO_2-TPD experiments were performed (Figure 8) where it can

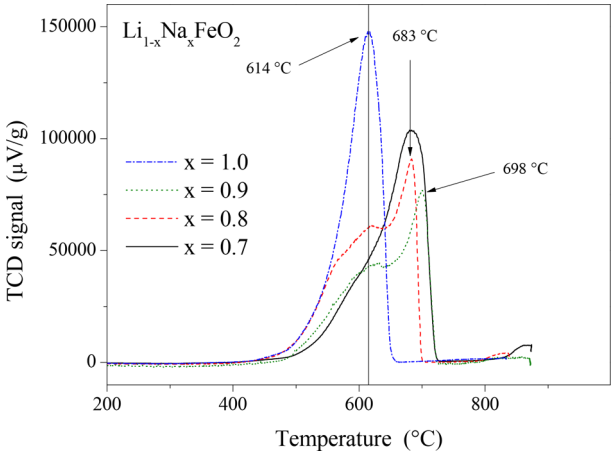

Figure 8. CO_2-TPD experiments for $NaFeO_2$, $Li_{0.1}Na_{0.9}FeO_2$, $Li_{0.2}Na_{0.8}FeO_2$, and $Li_{0.3}Na_{0.7}FeO_2$ samples under helium atmosphere.

be seen that the $NaFeO_2$ sample displayed a desorption process with a maximum TCD signal at 614 °C, which was 212 °C lower than the decarbonation process presented in Figure 7B. This temperature difference was due to the environmental atmosphere: as high CO_2 concentration increases, the decarbonation process moves at higher temperatures according with the Le Chatelier principle.

While the signal at 614 °C vanished as sodium content reached 70%, the $Li_{0.3}Na_{0.7}FeO_2$ sample showed a desorption process with a maximum TCD signal at 683 °C. This behavior agreed with the fact that the orthorhombic crystal phase ratio decreased as the rhombohedral phase took place as a major crystal phase in the $Li_{0.3}Na_{0.7}FeO_2$ sample. Thus, it must be correlated that CO_2 capture properties in this sample were mainly due to the rhombohedral crystal phase. Besides, this phase showed a CO_2 desorption process 70 °C above, compared to the orthorhombic phase. In addition, CO_2 capture in the cubic phase was neglected, and the orthorhombic weight fraction was near 4%.

Under this hypothesis, isothermal thermogravimetric experiments on $Li_{0.3}Na_{0.7}FeO_2$ and $NaFeO_2$ samples were performed to study kinetic CO_2 capture properties in both rhombohedral and orthorhombic crystal phases. Results of these experiments are shown in Figure 9, where it is possible to observe that the $Li_{0.3}Na_{0.7}FeO_2$ sample displayed a 5.5 wt % of CO_2 capture at 300 °C (Figure 9A), which was a higher value compared with those obtained in a dynamic experiment at the same temperature (1 wt %, in Figure 6). For the $Li_{0.3}Na_{0.7}FeO_2$ sample, CO_2 capture increased as a function of temperature until the gain mass reached 13.5 wt %, which was 65% of CO_2 theoretical capture (at 750 °C). Moreover, 65% CO_2 capture was close to 70% sodium content in nominal composition which implied that the rhombohedral crystal phase could be composed mainly by sodium ions.

Furthermore, isothermal thermogravimetric experiments on the $NaFeO_2$ sample (Figure 9B) showed a maximum of 17.5 wt % of CO_2 captured at 700 °C, which corresponded to 90% of the expected capture. At higher temperatures, maximum CO_2 capture displayed lower values due to the decarbonation process (data not shown). It is remarkable that the linear-like profile exhibited by isothermal experiments performed at 300 and 350 °C, which are substantially different from those made at higher temperatures. In fact, CO_2 capture at 300 °C was almost 2 wt %, which was lower than $Li_{0.3}Na_{0.7}FeO_2$ capture at the same physicochemical conditions (5.5 wt %). This fact could be related with a change in capture properties.

CO_2 capture cycling experiments were carried out on $Li_{0.3}Na_{0.7}FeO_2$ and $NaFeO_2$ samples in order to evaluate their performance against cyclability (Figure 10). In these experiments capture was done at 600 °C under a CO_2 flow (60 mL/min), while decarbonation was performed at 800 °C under N_2 flow (60 mL/min). Cycling experiments were not performed at constant temperature since decarbonation did not occur by gas

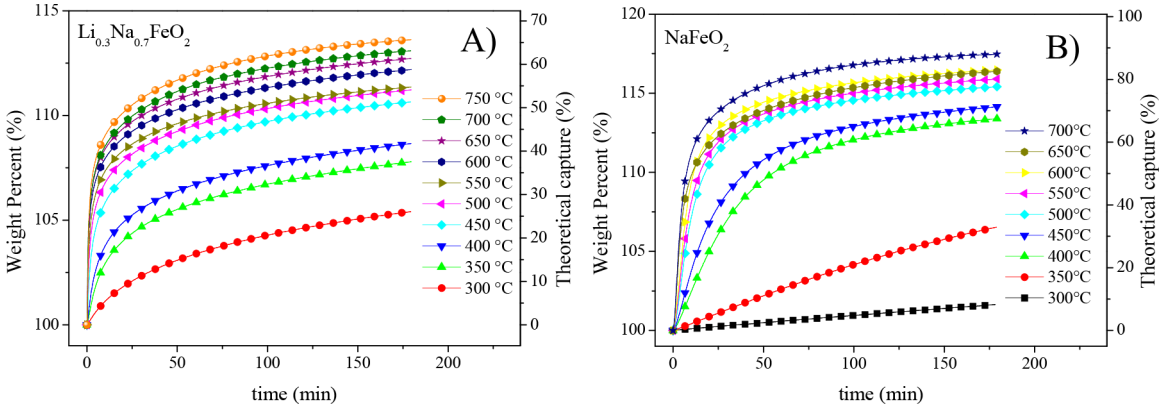

Figure 9. Isothermal thermogravimetric experiments for (A) $Li_{0.3}Na_{0.7}FeO_2$ and (B) $NaFeO_2$ samples under CO_2 atmosphere.

DOI: 10.1021/acs.jpcc.8b05578
J. Phys. Chem. C 2018, 122, 21162−21171

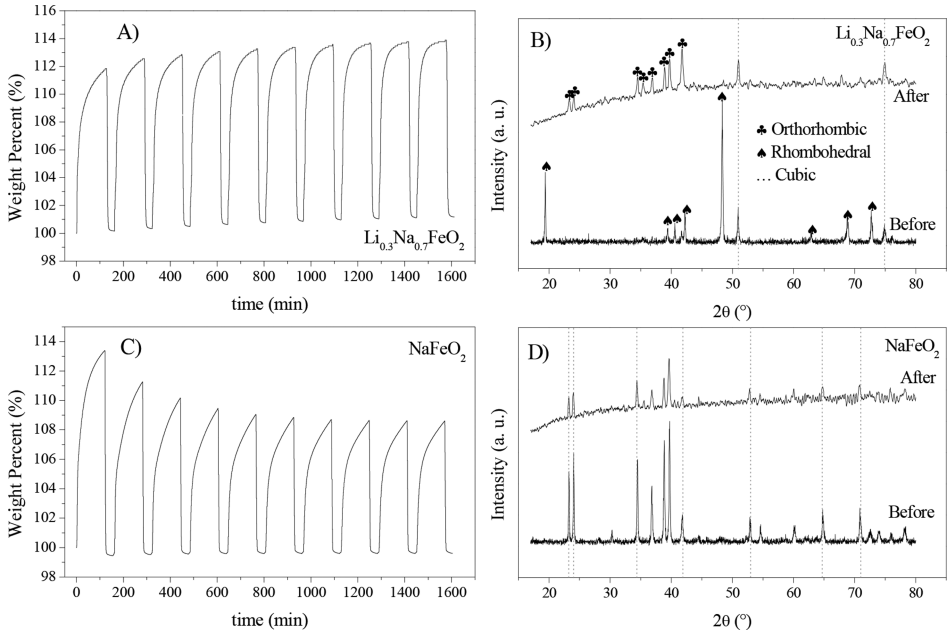

Figure 10. CO_2 capture−desorption (600−800 °C) cyclic tests for (A) $Li_{0.3}Na_{0.7}FeO_2$ and (C) $NaFeO_2$ samples. Also, X-ray diffraction patterns before and after cycling experiments are shown for (B) $Li_{0.3}Na_{0.7}FeO_2$ and (D) $NaFeO_2$ samples.

flow changing at 600 °C (data not shown). Figure 10A shows that CO_2 capture for the $Li_{0.3}Na_{0.7}FeO_2$ sample began with 11.8 wt %, and after ten cycles the maximum CO_2 capture remained constant, even increasing (12.6 wt %). In Figure 10B it is shown the X-ray diffraction patterns before and after the cycling experiments for $Li_{0.3}Na_{0.7}FeO_2$. At the beginning, this sample showed three crystal phases: cubic, rhombohedral, and orthorhombic (last one as traces), but after ten cycles the sample displayed only cubic and orthorhombic phases. Thus, the rhombohedral crystal phase disappeared, while the orthorhombic crystal phase became the majority phase.

Figure 10C displays CO_2 cycling capture of the $NaFeO_2$ sample, and it can be seen that the maximum capture started at 13.3 wt % but decreased to 8.7 wt % after seven cycles, before remaining constant. Moreover, X-ray diffraction patterns before and after cycling experiments (Figure 10D) showed the same crystal structure in the $NaFeO_2$ sample, indicating a complete regeneration after multiple CO_2 capture−decarbonation processes. Additionally, specific surface area was determinate, employing BET model on N_2 adsorption−desorption curves (data not shown). Results showed that initial specific surface areas were 1.69 and 1.52 m^2/g for $Li_{0.3}Na_{0.7}FeO_2$ and $NaFeO_2$ samples, respectively. After cycling, both samples decreased specific surface areas to 0.25 m^2/g for $Li_{0.3}Na_{0.7}FeO_2$ and 0.27 m^2/g for $NaFeO_2$. These values indicated that microstructure showed a small modification by cycling experiments compared with superficial sorbents, such as carbon-based materials for which specific surface areas around hundreds of times the values were shown by $Li_{0.3}Na_{0.7}FeO_2$ and $NaFeO_2$ samples.[45] The reduction in specific surface areas after cycling experiments agrees with a sintering process produced due to thermal conditions.

Kinetic CO_2 capture properties at different temperatures were related with chemical composition and crystal structure. Thus, CO_2 capture rate constants were obtained from the double exponential model (eq 4), and the Eyring model (eq 5) was further employed to obtain the activated-state enthalpies ($\Delta H^{\ddagger}$). Figure 11 presents rate constants in an Eyring-type

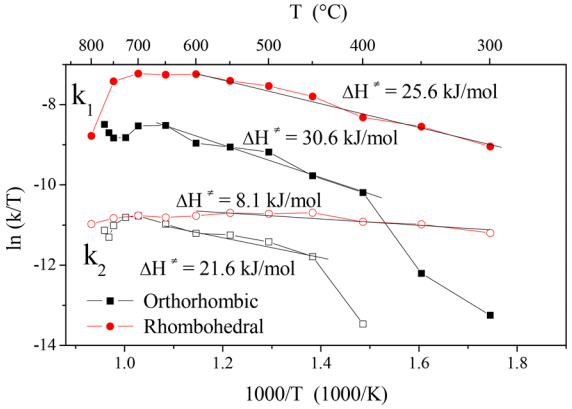

Figure 11. Eyring-type plots for CO_2 capture kinetic constants on $Li_{0.3}Na_{0.7}FeO_2$ and $NaFeO_2$ samples. Square symbols denote the rate constants obtained for $NaFeO_2$ with orthorhombic crystal phase. Circle symbols denote rate constants obtained for the $Li_{0.3}Na_{0.7}FeO_2$ sample with the rhombohedral crystal phase as a majority phase.

plot, where corresponding activated-state enthalpies for k_1 and k_2 of $Li_{0.3}Na_{0.7}FeO_2$ and $NaFeO_2$ samples are shown. From this figure, it is possible to observe that k_2 values were similar between both compositions, but k_1 values contrasted considerably. In this case, faster carbonation occurred in rhombohedral structure, where cations have octahedral coordination. From $Li_{0.97}Na_{0.03}FeO_2$ the kinetic study was settled that k_2 values were correlated with crystal structure, while k_1 values were correlated with chemical composition. Under this consideration, the resemblance in activated-state enthalpy obtained from k_1 values (25.6 and 30.6 kJ/mol for the $Li_{0.3}Na_{0.7}FeO_2$ and $NaFeO_2$ compositions, respectively) agreed with the fact that both compositions had high sodium content, and this species was mainly responsible for CO_2 capture on alkali-based ferrites.

Moreover, there was a considerable difference between the $\Delta H^{\ddagger}$ obtained from k_2 values for the above cited compositions, 8.1 kJ/mol for the rhombohedral crystal phase and 21.6 kJ/mol for the orthorhombic crystal phase. This higher value took place

DOI: 10.1021/acs.jpcc.8b05578
J. Phys. Chem. C 2018, 122, 21162−21171

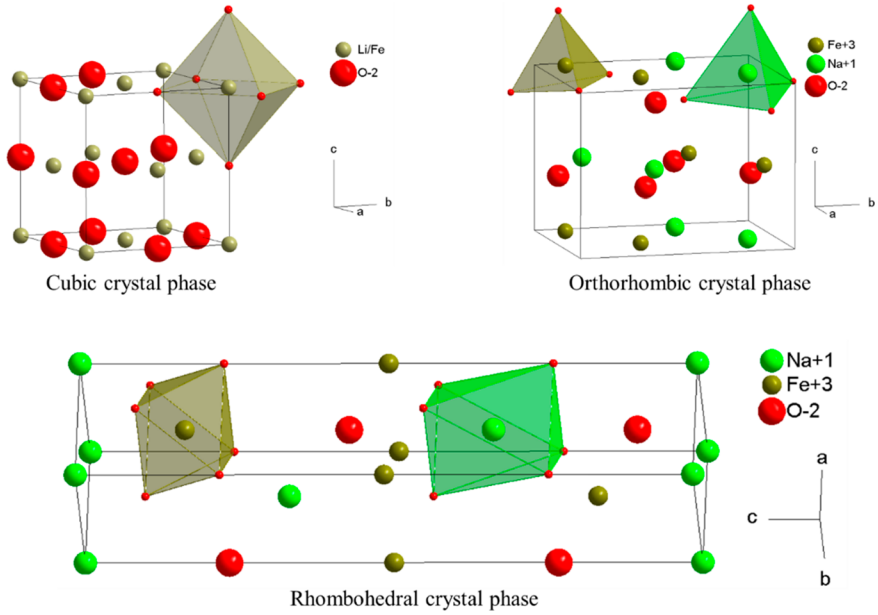

Figure 12. Crystal structures for different compositions studied in this work. Alkali-cation environment is octahedral in the cubic and rhombohedral crystal phases, while it is tetrahedral in the orthorhombic crystal phase.

in the crystal structure, where alkali cations had tetrahedral coordination with oxygen ions (orthorhombic crystal structure, Figure 12). The other two structures had an octahedral environment for alkali cations, but in all these structures alkali cations must pass through three oxygen ions to diffuse into the lattice and then react with CO_2. Oxygen anions form a triangle gap, which could be related with the activated-state enthalpy obtained for each structure. The triangle-gap area in this work was calculated using the formula of Heron, and the edge length for each triangle was calculated from the crystallographic data obtained from Rietveld refinement for each composition. Table 3 lists the calculated triangle-gap areas, and it is possible to see

Table 3. CO_2 Capture $\Delta H^{\ddagger}$ Values Obtained for All Compositions Studied in This Work and Their Relationship with the Alkali Crystal Environment

sample composition	$\Delta H^{\ddagger}$ composition-related (kJ/mol)	$\Delta H^{\ddagger}$ structure-related (kJ/mol)	alkali cation coordination	triangle-gap area (Å^2)
$LiFeO_2$	--	--	6	≈3.7
$Li_{0.97}Na_{0.03}FeO_2$	56.9	--	6	≈3.7
$Li_{0.94}Na_{0.06}FeO_2$	56.9	--	6	≈3.7
$Li_{0.3}Na_{0.7}FeO_2$	25.6	8.1	6	5.01
$NaFeO_2$	30.6	21.6	4	5.84

that the highest structure-related $\Delta H^{\ddagger}$ (21.6 kJ/mol) appeared in composition with only the orthorhombic crystal phase ($NaFeO_2$). In this sample, the calculated triangle-gap area was 5.84 Å^2. The $\Delta H^{\ddagger}$ value diminishes to 8.1 kJ/mol for the rhombohedral phase, which had only 5.01 Å^2 in the triangle gap. For lower area values, there was not an experimental $\Delta H^{\ddagger}$ value. Perhaps the gap was too narrow, where crystal diffusion was a nonfavored process.

The relation between the $\Delta H^{\ddagger}$ structure-related and triangle-gap area could be employed in analogous systems, such as $Li_{1+x}FeO_2$, where lithium ions are located into octahedral sites when $x = 0$. Additionally, when $x = 0.3$, lithium excess ions were placed into tetrahedral sites, and they reacted with CO_2; however, octahedral-coordinated lithium remained nonreacting.[30] In the $Li_{1+x}FeO_2$ system, it was possible to obtain a $\Delta H^{\ddagger}$ structure-related value of 36.1 kJ/mol only for the compound with 30% lithium excess, which has a similar quantity of lithium in tetrahedral sites. This value agreed with the $\Delta H^{\ddagger}$ value obtained for $NaFeO_2$ (21.6 kJ/mol, Table 3). Analogous to $Li_{1.3}FeO_2$, in the $NaFeO_2$ structure, sodium ions had a tetrahedral coordination. It would be said that the $\Delta H^{\ddagger}$ was higher for lithium-based ferrites than sodium-based ferrites; this value was related with diffusional process into the lattice, so a lithium ionic radius of 0.59 Å[46] must facilitate lithium diffusion compared with the larger sodium ionic radius (0.99 Å).[46] Moreover, the $\Delta H^{\ddagger}$ values obtained for $Li_{1.3}FeO_2$ and $NaFeO_2$ opposed this idea, which indicated that there was another characteristic changing this effect. Since there is a similarity in both coordination number and surrounding anions, the effects of electronegativity and the hardness were helpful concepts to understand $\Delta H^{\ddagger}$ values. The electronegativity for Li^+ and Na^+ ions is known as 40.52 and 26.21 eV,[47] respectively, indicating that Na−O interaction is more ionic than Li−O interaction. Analogously, hardness values for Li^+ and Na^+ are 35.12 and 21.08 eV, suggesting a strong hard−hard interaction in the Li−O bond. The higher hardness and lower ionic character in the Li−O bond suggested that, additionally to ionic contribution, this bond had a covalent contribution which needed more energy to be broken in order to diffuse lithium and then increase the $\Delta H^{\ddagger}$ value compared with the $NaFeO_2$ case.

Therefore, to improve CO_2 capture in alkali-based ferrites, the following characteristics should be considered: the relation between crystal structure and carbonation rate. Carbonation rates were higher in crystal structures, where alkali ions had an octahedral coordination (rhombohedral phase). This feature suggests that the $Li_{0.3}Na_{0.7}FeO_2$ sample is suitable to capture CO_2 at intermediate temperatures. Another important characteristic is the relation of $\Delta H^{\ddagger}$ value with temperature. The rhombohedral phase had the lowest $\Delta H^{\ddagger}$ values, which implied that CO_2 capture was slightly affected by increasing temperature.

DOI: 10.1021/acs.jpcc.8b05578
J. Phys. Chem. C 2018, 122, 21162−21171

However, in the orthorhombic phase, where alkali ions have a tetrahedral coordination, $\Delta H^{\ddagger}$ values were higher, involving a strong temperature dependency, making $NaFeO_2$ a suitable material for CO_2 capture at high temperatures.

CONCLUSIONS

In this work, several compositions were synthesized that belong to the $Li_{1-x}Na_xFeO_2$ system by nitrate decomposition, using low and short thermal treatments. The compositions in which sodium content were less than 6% (mole fraction) displayed a cubic single phase. On the contrary, the 100% sodium composition presented an orthorhombic single phase, while intermediate compositions showed mixtures in which a rhombohedral phase coexisted between $0.1 < x < 0.9$ values. The rhombohedral phase was the major phase at $x = 0.7$ composition. Concerning to CO_2 capture, the kinetic CO_2 capture studies on compounds with cubic structure allowed us to identify that k_1 and k_2 rate constants are related with the chemical composition and the crystal structure, respectively. Despite the high alkali content in the cubic phase compositions, these are not suitable for CO_2 capture. Moreover, the $NaFeO_2$ compound showed a 90% efficiency in CO_2 capture at 700 °C with $\Delta H^{\ddagger}$ values of 30.6 and 21.6 kJ/mol for composition and structural CO_2 capture-related processes, respectively. In spite of the high capture efficiency showed by the $NaFeO_2$ composition, the faster carbonation reaction took place in the $Li_{0.3}Na_{0.7}FeO_2$ composition, which displays a rhombohedral crystal phase as a main phase. This composition showed a 65% efficiency in CO_2 capture at 750 °C, and this capture percent is comparable with its sodium content. Furthermore, $Li_{0.3}Na_{0.7}FeO_2$ presented the best CO_2 cycling behavior.

TPD experiments showed that the decarbonation process in this composition was different from the $NaFeO_2$ compound, and then, this process was associated with the rhombohedral crystal phase. Additionally, the decarbonation process took place at temperatures above 700 °C for the $NaFeO_2$ compound, whereas the same process took place at 750 °C in the $Li_{0.3}Na_{0.7}FeO_2$ composition. Also, for this sample $\Delta H^{\ddagger}$ values were 25.6 and 8.1 kJ/mol for the composition and structural CO_2 capture-related process, respectively, which were related only to the rhombohedral phase. Finally, CO_2 capture was associated with a triangle gap that oxygen anions make around alkali ions. It was found that if the triangle gap is narrow (3.7 $Å^2$ in cubic phase) CO_2 capture is neglected. However, if the triangle gap is wide (5 $Å^2$ or higher) the compositions were able to capture large amounts of CO_2, 13.5 and 17.5 wt % for rhombohedral and orthorhombic crystal phases, respectively. Also, the structural-related $\Delta H^{\ddagger}$ was associated with bonding properties, finding that a covalent contribution increases the $\Delta H^{\ddagger}$ values in CO_2 capture.

AUTHOR INFORMATION

Corresponding Author

*Phone: +52 (55) 5622 4656. E-mail: jfrancisco@comunidad.unam.mx.

ORCID

J. Francisco Gómez-García: 0000-0003-1309-7190

Heriberto Pfeiffer: 0000-0002-6217-3420

Notes

The authors declare no competing financial interest.

ACKNOWLEDGMENTS

JFGG thanks the "Programa de Becas Posdoctorales, UNAM" for the scholarship granted. Authors thank projects PAPIIT-UNAM (IN-101916) and SENER-CONACYT (251801) for financial support.

REFERENCES

(1) Li, B.; Duan, Y.; Luebke, D.; Morreale, B. Advances in CO_2 Capture Technology: A Patent Review. *Appl. Energy* **2013**, *102*, 1439–1447.

(2) Spigarelli, B. P.; Kawatra, S. K. Opportunities and Challenges in Carbon Dioxide Capture. *J. CO2 Util* **2013**, *1*, 69–87.

(3) Pires, J. C. M.; Martins, F. G.; Alvim-Ferraz, M. C. M.; Simões, M. Recent Developments on Carbon Capture and Storage: An Overview. *Chem. Eng. Res. Des.* **2011**, *89*, 1446–1460.

(4) MacDowell, N.; Florin, N.; Buchard, A.; Hallett, J.; Galindo, A.; Jackson, G.; Adjiman, C. S.; Williams, C. K.; Shah, N.; Fennell, P. An Overview of CO_2 Capture Technologies. *Energy Environ. Sci.* **2010**, *3*, 1645.

(5) Boot-Handford, M. E.; Abanades, J. C.; Anthony, E. J.; Blunt, M. J.; Brandani, S.; Mac Dowell, N.; Fernández, J. R.; Ferrari, M.-C.; Gross, R.; Hallett, J. P.; et al. Carbon Capture and Storage Update. *Energy Environ. Sci.* **2014**, *7*, 130–189.

(6) Wee, J.-H. Carbon Dioxide Emission Reduction Using Molten Carbonate Fuel Cell Systems. *Renewable Sustainable Energy Rev.* **2014**, *32*, 178–191.

(7) Zhang, X.; Zhang, X.; Dong, H.; Zhao, Z.; Zhang, S.; Huang, Y. Carbon Capture with Ionic Liquids: Overview and Progress. *Energy Environ. Sci.* **2012**, *5*, 6668.

(8) Yu, C.-H.; et al. A Review of CO2 Capture by Absorption and Adsorption. *Aerosol Air Qual. Res.* **2012**, *12*, 745.

(9) Wang, Q.; Luo, J.; Zhong, Z.; Borgna, A. CO_2 Capture by Solid Adsorbents and Their Applications: Current Status and New Trends. *Energy Environ. Sci.* **2011**, *4*, 42–55.

(10) Martínez-dlCruz, L.; Pfeiffer, H. Toward Understanding the Effect of Water Sorption on Lithium Zirconate (Li_2ZrO_3) during Its Carbonation Process at Low Temperatures. *J. Phys. Chem. C* **2010**, *114*, 9453–9458.

(11) Ortiz-Landeros, J.; Martínez-dlCruz, L.; Gómez-Yáñez, C.; Pfeiffer, H. Towards Understanding the Thermoanalysis of Water Sorption on Lithium Orthosilicate (Li_4SiO_4). *Thermochim. Acta* **2011**, *515*, 73–78.

(12) Rodríguez-Mosqueda, R.; Pfeiffer, H. High CO_2 Capture in Sodium Metasilicate (Na_2SiO_3) at Low Temperatures (30–60 °C) through the CO_2–H_2O Chemisorption Process. *J. Phys. Chem. C* **2013**, *117*, 13452–13461.

(13) Kumar, S.; Saxena, S. K. A Comparative Study of CO_2 Sorption Properties for Different Oxides. *Mater. Renew. Sustain. Energy* **2014**, *3*, 30.

(14) Mosqueda, H. A.; Vazquez, C.; Bosch, P.; Pfeiffer, H. Chemical Sorption of Carbon Dioxide (CO_2) on Lithium Oxide (Li_2O). *Chem. Mater.* **2006**, *18*, 2307–2310.

(15) Pfeiffer, H.; Bosch, P. Thermal Stability and High-Temperature Carbon Dioxide Sorption on Hexa-Lithium Zirconate ($Li_6Zr_2O_7$). *Chem. Mater.* **2005**, *17*, 1704–1710.

(16) Alcérreca-Corte, I.; Fregoso-Israel, E.; Pfeiffer, H. CO_2 Absorption on Na_2ZrO_3: A Kinetic Analysis of the Chemisorption and Diffusion Processes. *J. Phys. Chem. C* **2008**, *112*, 6520–6525.

(17) Ochoa-Fernández, E.; Rønning, M.; Grande, T.; Chen, D. Synthesis and CO_2 Capture Properties of Nanocrystalline Lithium Zirconate. *Chem. Mater.* **2006**, *18*, 6037–6046.

(18) Duan, Y.; Lekse, J. Regeneration Mechanisms of High-Lithium Content Zirconates as CO_2 Capture Sorbents: Experimental Measurements and Theoretical Investigations. *Phys. Chem. Chem. Phys.* **2015**, *17*, 22543–22547.

(19) Rodríguez, M. T.; Pfeiffer, H. Sodium Metasilicate (Na_2SiO_3): A Thermo-Kinetic Analysis of Its CO_2 Chemical Sorption. *Thermochim. Acta* **2008**, *473*, 92–95.

DOI: 10.1021/acs.jpcc.8b05578
J. Phys. Chem. C 2018, 122, 21162–21171

(20) Mizunuma, M.; Tsuda, M.; Maruo, Y.; Nakagaki, T. CO_2 Capture System Using Lithium Silicate for Distributed Power Supply. *Energy Procedia* **2013**, *37*, 1194−1201.
(21) Sanna, A.; Maroto-Valer, M. M. CO_2 Capture at High Temperature Using Fly Ash-Derived Sodium Silicates. *Ind. Eng. Chem. Res.* **2016**, *55*, 4080−4088.
(22) Palacios-Romero, L. M.; Lima, E.; Pfeiffer, H. Structural Analysis and CO_2 Chemisorption Study on Nonstoichiometric Lithium Cuprates ($Li_{2+X}CuO_{2+x/2}$). *J. Phys. Chem. A* **2009**, *113*, 193−198.
(23) Ávalos-Rendón, T.; Casa-Madrid, J.; Pfeiffer, H. Thermochemical Capture of Carbon Dioxide on Lithium Aluminates ($LiAlO_2$ and Li_5AlO_4): A New Option for the CO_2 Absorption. *J. Phys. Chem. A* **2009**, *113*, 6919−6923.
(24) Sánchez-Camacho, P.; Romero-Ibarra, I. C.; Duan, Y.; Pfeiffer, H. Thermodynamic and Kinetic Analyses of the CO_2 Chemisorption Mechanism on Na_2TiO_3: Experimental and Theoretical Evidences. *J. Phys. Chem. C* **2014**, *118*, 19822−19832.
(25) López-Ortiz, A.; Rivera, N. G. P.; Rojas, A. R.; Gutierrez, D. L. Novel Carbon Dioxide Solid Acceptors Using Sodium Containing Oxides. *Sep. Sci. Technol.* **2005**, *39*, 3559−3572.
(26) Lara-García, H. A.; Sanchez-Camacho, P.; Duan, Y.; Ortiz-Landeros, J.; Pfeiffer, H. Analysis of the CO2 Chemisorption in Li_5FeO_4, a New High Temperature CO_2 Captor Material. Effect of the CO2 and O2 Partial Pressures. *J. Phys. Chem. C* **2017**, *121*, 3455−3462.
(27) Yanase, I.; Kameyama, A.; Kobayashi, H. CO_2 Absorption and Structural Phase Transition of α-$LiFeO_2$. *J. Ceram. Soc. Jpn.* **2010**, *118*, 48−51.
(28) Eba, H.; Sakurai, K. Enhancement of CO_2 Absorbance for Lithium Ferrite-Combinatorial Application of X-Ray Absorption Fine Structure Imaging. *Mater. Trans.* **2005**, *46*, 665−668.
(29) Yanase, I.; Otzuka, H.; Kobayashi, H. CO_2 Absorption of CeO_2-Coated α-$LiFeO_2$. *J. Ceram. Soc. Jpn.* **2011**, *119*, 933−938.
(30) Gomez-Garcia, J. F.; Pfeiffer, H. Structural and CO_2 Capture Analyses of the $Li_{1+x}FeO_2$ ($0 \leq x \leq 0.3$) System: Effect of Different Physicochemical Conditions. *RSC Adv.* **2016**, *6*, 112040−112049.
(31) Lara-García, H. A.; Vera, E.; Mendoza-Nieto, J. A.; Gómez-García, J. F.; Duan, Y.; Pfeiffer, H. Bifunctional Application of Lithium Ferrites (Li_5FeO_4 and $LiFeO_2$) during Carbon Monoxide (CO) Oxidation and Chemisorption Processes. A Catalytic, Thermogravimetric and Theoretical Analysis. *Chem. Eng. J.* **2017**, *327*, 783−791.
(32) Blesa, M. C.; Moran, E.; León, C.; Santamaria, J.; Tornero, J. D.; Menéndez, N. α-$NaFeO_2$: Ionic Conductivity and Sodium Extraction. *Solid State Ionics* **1999**, *126*, 81−87.
(33) Grey, I. E.; Hill, R. J.; Hewat, A. W. A Neutron Powder Diffraction Study of the β to γ Phase Transformation in $NaFeO_2$. *Zeitschrift für Krist* **1990**, *193*, 51−69.
(34) Grey, I. E.; Li, C. New Silica-Containing Ferrite Phases in the System $NaFeO_2$-SiO_2. *J. Solid State Chem.* **1987**, *69*, 116−125.
(35) Larson, A. C.; Von Dreele, R. B. *General Structure Analysis System (GSAS)*. Los Alamos National Laboratory Report LAUR 86−748; 1994.
(36) Toby, B. H. EXPGUI, a Graphical User Interface for GSAS. *J. Appl. Crystallogr.* **2001**, *34*, 210−213.
(37) Bertaut, F.; Blum, P. Structure d'une Nouvelle Variete de Ferrite de Sodium ($FeNaO_2$). *C. R. Hebd. Seances Acad. Sci.* **1954**, *239*, 429−431.
(38) McQueen, T.; Huang, Q.; Lynn, J. W.; Berger, R. F.; Klimczuk, T.; Ueland, B. G.; Schiffer, P.; Cava, R. J. Magnetic Structure and Properties of the S = 5/2 Triangular Antiferromagnet A−$NaFeO_2$. *Phys. Rev. B: Condens. Matter Mater. Phys.* **2007**, *76*, 024420.
(39) Ávalos-Rendón, T.; Pfeiffer, H. Evidence of CO_2 Chemisorption at High Temperature in Lithium Gallate (Li_5GaO_4). *Chem. Lett.* **2011**, *40*, 504−505.
(40) Alcántar-Vázquez, B.; Diaz, C.; Romero-Ibarra, I. C.; Lima, E.; Pfeiffer, H. Structural and CO_2 Chemisorption Analyses on $Na_2(Zr_{1-x}Al_x)O_3$ Solid Solutions. *J. Phys. Chem. C* **2013**, *117*, 16483−16491.
(41) Rodríguez-Mosqueda, R.; Pfeiffer, H. Thermokinetic Analysis of the CO_2 Chemisorption on Li_4SiO_4 by Using Different Gas Flow Rates and Particle Sizes. *J. Phys. Chem. A* **2010**, *114*, 4535−4541.
(42) Eyring, H. The Activated Complex in Chemical Reactions. *J. Chem. Phys.* **1935**, *3*, 107−115.
(43) Eyring, H. The Activated Complex and the Absolute Rate of Chemical Reactions. *Chem. Rev.* **1935**, *17*, 65−77.
(44) Laidler, K. J.; King, M. C. Development of Transition-State Theory. *J. Phys. Chem.* **1983**, *87*, 2657−2664.
(45) Plaza, M. G.; Pevida, C.; Arenillas, A.; Rubiera, F.; Pis, J. J. CO_2 Capture by Adsorption with Nitrogen Enriched Carbons. *Fuel* **2007**, *86*, 2204−2212.
(46) Shannon, R. D. Revised Effective Ionic Radii and Systematic Studies of Interatomic Distances in Halides and Chalcogenides. *Acta Crystallogr., Sect. A: Cryst. Phys., Diffr., Theor. Gen. Crystallogr.* **1976**, *32*, 751−767.
(47) Pearson, R. G. Absolute Electronegativity and Hardness: Application to Inorganic Chemistry. *Inorg. Chem.* **1988**, *27*, 734−740.

DOI: 10.1021/acs.jpcc.8b05578
J. Phys. Chem. C 2018, 122, 21162−21171